

Discrete Fourier Analysis of Images of Structural Defects in Single Crystals

I. A. Zhukovskaya^a, V. A. Bushuev^b, and V. A. Tkal^a

^aVeliky Novgorod Branch, St. Petersburg State University of Economics, Veliky Novgorod, Novgorod oblast, 173000 Russia

^bMoscow State University, Moscow, 119991 Russia

e-mail: Valery.Tkal@yandex.ru

Received May 20, 2015

Abstract—The absolute value and argument of discrete Fourier transform (DFT) coefficients are investigated by analyzing images of test objects and structural defects in single crystals, which are theoretically calculated from modified Indenbom–Chamrov equations and experimental data. The role of the argument of DFT coefficients is demonstrated in revealing the peculiarities of the contrast generated by structural defects and their reliable identification and localization in the bulk of a single crystal.

Keywords: X-ray topography, defect imaging, theoretical and experimental contrasts, test objects, Fourier analysis, digital image processing

DOI: 10.1134/S1027451015060403

INTRODUCTION

The identification of structural defects and their localization within the bulk of single crystals is one of the greatest problems of physical materials science. The most widespread diagnostic methods are X-ray topographic and polarization-optical analyses. Among the topographic methods, it is possible to highlight X-ray topography based on the Borrmann effect, which exhibited good results in studying low-dislocation-density and dislocation-free materials [1]. In this method, the contrast formed by the structural defects of single crystals has the form of intensity rosettes. In this case, the shape and number of petals thereof depends heavily on the defect type and its arrangement in the single-crystal bulk, and the sizes are determined by the single-crystal type. Structural-defect identification is simplified by the fact that the theoretical contrast thereof can be simulated from modified Indenbom–Chamrov equations [1] and the digital processing of experimental contrast. The latter is intended to enhance its quality and remove the main noise-induced factors, such as low-level contrast, background inhomogeneity, and photoemulsion graininess.

Digital processing of the contrast can be based on the brightness and frequency characteristics of the contrast under analysis, i.e., involve wavelet and Fourier transforms [2–4]. In [2], main focus was placed on the digital processing of topographic and polarization-optical contrasts of promising materials in electronic engineering, which contain images of structural imperfections of different types, with the help of digital methods relying on the analysis of brightness char-

acteristics and the wavelet transform. Moreover, the authors demonstrated the possibility of increasing the reliability and unambiguity of identifying different structural imperfections. In [3, 4], the problem of recovery of the internal structure of weakly absorbing objects using X-ray phase-contrast data and analysis of the influence of statistical noise on the recovery accuracy by means of the Fourier transform was considered.

This work is the logical continuation of studies of authors devoted to the digital processing of defects in crystalline structures and considers Fourier analysis of the contrast as applied to achieving the aforementioned purpose.

FOURIER FILTERING OF A DISCRETE IMAGE

Images of topographic and polarization-optical contrasts can be qualitatively improved via Fourier filtering of a discrete image. It is assumed that the Fourier filtering algorithm includes the discrete Fourier transform (DFT), a correction to the DFT coefficients, and image reconstruction (i.e., recovery) via the inverse DFT [1]. Filtered images contain most of the main characteristics of the initial image, enabling us to rather reliably identify imperfections in the structure of a single crystal. In so doing, only the absolute values of the complex coefficients of the DFT are corrected, and their arguments remain unchanged.

The contrast (image) analyzed can be interpreted as a real function of two variables $f(x, y)$. Therefore,

with the use of the DFT, the aperiodic 2D real sequence

$$\{f(j_x, j_y)\}, \quad 0 \leq j_x \leq N_x - 1, \quad 0 \leq j_y \leq N_y - 1, \quad (1)$$

which is created from values of function $f(x, y)$ at equidistant nodes (x_{j_x}, y_{j_y}) of a rectangular mesh with the quantization steps $\Delta x, \Delta y$, should be transformed by adding zero samples to a periodic sequence with the period $N_1 \times N_2$:

$$f_p(j_x, j_y) = \begin{cases} f(j_x, j_y), & \begin{cases} 0 \leq j_x \leq N_x - 1, \\ 0 \leq j_y \leq N_y - 1, \end{cases} \\ 0, & \text{in other cases,} \end{cases} \quad (2)$$

Here, $j_x = 0, 1, 2, \dots, N_1 - 1, j_y = 0, 1, 2, \dots, N_2 - 1, N_1 = \min_m \{2^m \geq N_x\}, N_2 = \min_m \{2^m \geq N_y\}$, are the periods of the indices j_x and j_y , respectively.

The periodic 2D real and complex sequences $\{f_p(j_x, j_y)\}$ and $\{F_p(l_x, l_y)\}$, respectively, satisfy the DFT:

$$F_p(l_x, l_y) = (1/N_1 N_2) \sum_{j_x=0}^{N_1-1} \sum_{j_y=0}^{N_2-1} f_p(j_x, j_y) \times \exp[-i2\pi(j_x l_x + j_y l_y)/N_1 N_2], \quad (3)$$

where $i = (-1)^{1/2}$ is the imaginary unit, $l_x = 0, 1, 2, \dots, N_1 - 1, l_y = 0, 1, 2, \dots, N_2 - 1$; and the DFT coefficients of the indices l_x and l_y have the periods N_1 , and N_2 , respectively.

The DFT coefficients can be filtered as follows:

$$F_{pw}(l_x, l_y) = W_p(l_x, l_y) F_p(l_x, l_y) = W_p(l_x, l_y) |F_p(l_x, l_y)| \exp[i \arg(F_p(l_x, l_y))], \quad (4)$$

where $W_p(l_x, l_y)$ is the real filtering multiplier. Hence, the absolute value and argument of the corrected DFT coefficients are expressed as

$$|F_{pw}(l_x, l_y)| = W_p(l_x, l_y) |F_p(l_x, l_y)|, \quad (5)$$

$$\arg(F_{pw}(l_x, l_y)) = \arg(F_p(l_x, l_y)). \quad (6)$$

For the periodic 2D sequences of complex and real functions designated respectively by $\{F_{pw}(l_x, l_y)\}$ and $\{f_{pw}(j_x, j_y)\}$ the inverse DFT is valid:

$$f_{pw}(j_x, j_y) = \sum_{l_x=0}^{N_1-1} \sum_{l_y=0}^{N_2-1} F_{pw}(l_x, l_y) \exp[i2\pi(l_x j_x + l_y j_y)/N_1 N_2]. \quad (7)$$

Afterward, a discrete filtered image is generated, namely,

$$f_w(j_x, j_y) = f_{pw}(j_x, j_y), \quad (8)$$

where $j_x = 0, 1, 2, \dots, N_x - 1, j_y = 0, 1, 2, \dots, N_y - 1$.

The Fourier filtering of a discrete image can be performed using the fast Fourier-transform algorithm by means of the Mathcad mathematical package involving built-in functions of the forward and inverse DFTs [5–7]. Function $\text{CFFT}(f)$ calculates the 2D forward DFT of an $N_1 \times N_2$, real matrix. The calculated result is an $N_1 \times N_2$, complex matrix of DFT coefficients. Function $\text{ICFFT}(F)$ calculates the 2D inverse DFT of an $N_1 \times N_2$, complex matrix of DFT coefficients. The calculated result is an $N_1 \times N_2$, real matrix. The functions $\text{CFFT}(f)$ and $\text{ICFFT}(F)$ are inverse to each other:

$$\text{ICFFT}(\text{CFFT}(f)) = f. \quad (9)$$

In the case where diffraction-contrast-formation theory was investigated by the example of ordinary photographic images, the author of [8] presented data on how a 2D signal phase behaves during its Fourier analysis and demonstrated that the signal phase contains important information on the image structure and is responsible for the transmission of the main distinctive features enabling its identification. In the example under study, the Fourier analysis of two photographs (images 1 and 2) was accompanied by image recovery based on combined coefficients; i.e., phase and amplitude coefficients taken from images 1 and 2, respectively. Upon recovery, image 1 was constructed, but the detail in terms of the brightness characteristics thereof was somewhat worse.

Let us consider the proposed approach to image reconstruction by the example of structural-defect identification based on the technique whereby the noise contamination of a theoretical contrast is fitted to an experimental contrast with subsequent digital processing [9]. Let us try to reveal what role is played by the phase (argument of complex DFT coefficients) in reconstructing the topographic and polarization-optical images via a procedure incorporating test images, the kind, sizes, and mutual positions of which are primarily different with the subsequent transference of structural defects to the theoretical and experimental contrasts.

ROLE OF THE ARGUMENT OF DFT COEFFICIENTS IN THE CASE OF THE FOURIER TRANSFORM OF TEST IMAGES

Two $N_x \times N_y$ 8-bit contrasts with object images differing in shape, size, intensity, background intensity, and with different variants of mutual arrangement were chosen as test objects. Forward and inverse DFT were carried out for each contrast, and reconstruction

Table 1. Results of the Fourier transform of test objects with similar shapes

No.	Contrast 1 $I_{\max} = 166, I_{\min} = 64$	Contrast 2 $I_{\max} = 217, I_{\min} = 127$	Reconstruction 12 (absolute values of and arguments of coefficients belonging to contrasts 1 and 2, respectively)	Reconstruction 21 (absolute values and arguments of coefficients belonging to contrasts 2 and 1, respectively)
1				
2				
3				
4				
5				
6				
7				

assumed the use of absolute values of the DFT coefficients of one contrast and their arguments of the other. The results of the given processing are presented in Tables 1–4, where the 8-bit image is characterized by the intensity I of gray gradation.

The contrasts under analysis can be interpreted as two-variable functions $f_1(x, y)$ and $f_2(x, y)$. In this



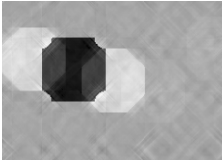





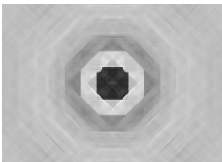
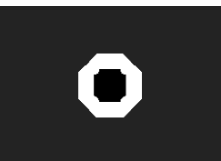

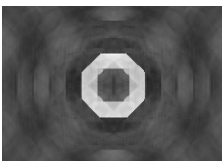
case, with the use of the DFT, the aperiodic 2D real sequences

$$\{f_1(j_x, j_y)\}, \quad 0 \leq j_x \leq N_x - 1, \quad 0 \leq j_y \leq N_y - 1, \quad (10)$$

$$\{f_2(j_x, j_y)\}, \quad 0 \leq j_x \leq N_x - 1, \quad 0 \leq j_y \leq N_y - 1, \quad (11)$$

which are generated from the values of functions $f_1(x, y)$ and $f_2(x, y)$ at the equidistant nodes (x_{j_x}, y_{j_y}) of a rect-

Table 2. Results of the Fourier transform of test objects with similar shapes and sizes under the condition of partially and completely overlapped images

No.	Contrast 1	Contrast 2	Reconstruction 12 (absolute values and arguments of coefficients belonging to contrasts 1 and 2, respectively)
1			
2			
3			
4			

angular mesh with the quantization steps $\Delta x, \Delta y$, should be transformed by adding zero samples into the periodic sequences with the period $N_1 \times N_2$:

$$f_{1p}(j_x, j_y) = \begin{cases} f_1(j_x, j_y), & \begin{cases} 0 \leq j_x \leq N_x - 1, \\ 0 \leq j_y \leq N_y - 1, \end{cases} \\ 0, & \text{in other cases,} \end{cases} \quad (12)$$

$$f_{2p}(j_x, j_y) = \begin{cases} f_2(j_x, j_y), & \begin{cases} 0 \leq j_x \leq N_x - 1, \\ 0 \leq j_y \leq N_y - 1, \end{cases} \\ 0, & \text{in other cases.} \end{cases} \quad (13)$$

Here, $j_x = 0, 1, 2, \dots, N_1 - 1, j_y = 0, 1, 2, \dots, N_2 - 1$; $N_1 = \min_m \{2^m \geq N_x\}$, $N_2 = \min_m \{2^m \geq N_y\}$, and N_1 , and N_2 are the periods of indices j_x and j_y , respectively.

Each pair of periodic 2D sequences of real and complex functions (i.e., $\{f_{1p}(j_x, j_y)\}$ and $\{F_{1p}(l_x, l_y)\}$, respectively), as well as the real and complex

sequences designated respectively by $\{f_{2p}(j_x, j_y)\}$ and $\{F_{2p}(l_x, l_y)\}$, obey the DFTs:

$$F_{1p}(l_x, l_y) = (1/N_1 N_2) \sum_{j_x=0}^{N_1-1} \sum_{j_y=0}^{N_2-1} f_{1p}(j_x, j_y) \times \exp[-i2\pi(j_x l_x + j_y l_y)/N_1 N_2], \quad (14)$$

$$F_{2p}(l_x, l_y) = (1/N_1 N_2) \sum_{j_x=0}^{N_1-1} \sum_{j_y=0}^{N_2-1} f_{2p}(j_x, j_y) \times \exp[-i2\pi(j_x l_x + j_y l_y)/N_1 N_2]. \quad (15)$$

Here, $i = (-1)^{1/2}$ is an imaginary unit, $l_x = 0, 1, 2, \dots, N_1 - 1, l_y = 0, 1, 2, \dots, N_2 - 1$; and N_1 , and N_2 are the periods of the DFT coefficients of indices l_x and l_y , respectively.



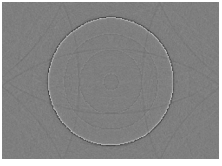
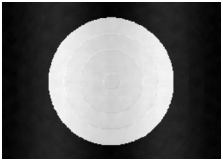
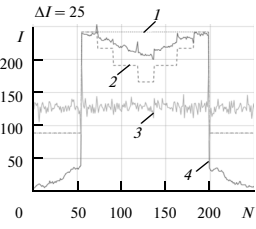


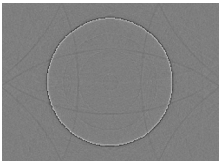

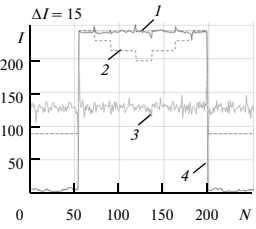


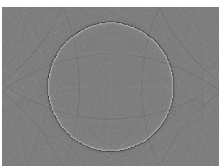
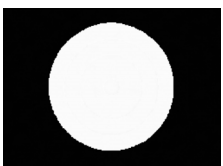
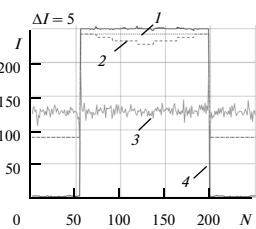


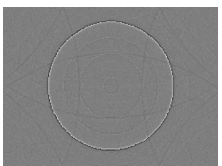
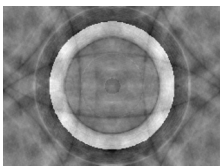
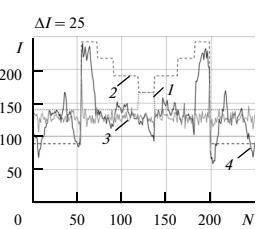
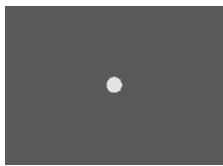

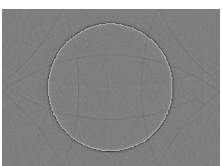
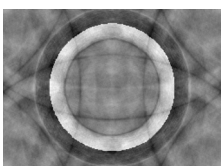
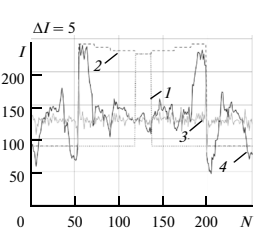
The DFT coefficients of the first and second contrasts can be combined as follows:

$$F_{p12}(l_x, l_y) = |F_{1p}(l_x, l_y)| \exp[i \arg(F_{2p}(l_x, l_y))], \quad (16)$$

or

$$F_{p21}(l_x, l_y) = |F_{2p}(l_x, l_y)| \exp(i \arg(F_{1p}(l_x, l_y))). \quad (17)$$

Table 3. Results of the Fourier transform of centered test objects with similar shapes, different sizes, and the contrasts of different intensity under the condition of complete overlapping

No.	Contrast 1 (IP 1)	Contrast 2 (IP 2)	Reconstruction 1 (absolute values and arguments of co- efficients belonging to contrasts 1 and 2, respectively) (IP 3)	Reconstruction 2 (absolute values and arguments of co- efficients belonging to contrasts 1 and 2, respectively) (IP 4)	IP 1–4
1	$I_0 = 89, I_1 = 242$ 	$\Delta I = 25, I_0 = 89,$ $I_1 = 242, I_2 = 217,$ $I_3 = 191, I_4 = 166$ 			
2	$I_0 = 89, I_1 = 242$ 	$\Delta I = 15, I_0 = 89,$ $I_1 = 242, I_2 = 227,$ $I_3 = 212, I_4 = 197$ 			
3	$I_0 = 89, I_1 = 242$ 	$\Delta I = 5, I_0 = 89,$ $I_1 = 242, I_2 = 237,$ $I_3 = 232, I_4 = 227$ 			
4	$I_0 = 140, I_1 = 166$ 	$\Delta I = 25, I_0 = 89,$ $I_1 = 242, I_2 = 217,$ $I_3 = 191, I_4 = 166$ 			
5	$I_0 = 89, I_1 = 227$ 	$\Delta I = 5, I_0 = 89,$ $I_1 = 242, I_2 = 237,$ $I_3 = 232, I_4 = 227$ 			

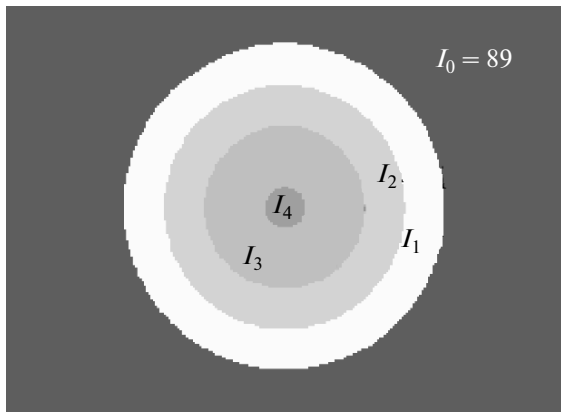


Fig. 1. Example of the numbering of circular centered intensities in the test contrast from Table 3. The intensity-level step is $\Delta I = 25$. $I_1 = 242$, $I_2 = 217$, $I_3 = 191$, $I_4 = 166$.

For two pairs of the periodic 2D sequences of complex and real functions designated respectively by $\{F_{p12}(l_x, l_y)\}$ and $\{f_{p12}(j_x, j_y)\}$, and complex and real sequences $\{F_{p21}(l_x, l_y)\}$ and $\{f_{p21}(j_x, j_y)\}$ respectively, the inverse DFTs are valid:

$$f_{p12}(j_x, j_y) = \sum_{l_x=0}^{N_1-1} \sum_{l_y=0}^{N_2-1} F_{p12}(l_x, l_y) \exp[i2\pi(l_x j_x + l_y j_y)/N_1 N_2], \quad (18)$$

$$f_{p21}(j_x, j_y) = \sum_{l_x=0}^{N_1-1} \sum_{l_y=0}^{N_2-1} F_{p21}(l_x, l_y) \exp[i2\pi(l_x j_x + l_y j_y)/N_1 N_2]. \quad (19)$$

After, discrete processed images are formed, namely,

$$f_{12}(j_x, j_y) = f_{p12}(j_x, j_y), \quad (20)$$

$$f_{21}(j_x, j_y) = f_{p21}(j_x, j_y), \quad (21)$$

where $j_x = 0, 1, 2, \dots, N_x - 1$, $j_y = 0, 1, 2, \dots, N_y - 1$.

ROLE OF THE ARGUMENT OF THE DFT COEFFICIENTS IN THE CASE OF THE FOURIER TRANSFORM OF A TEST CONTRAST

Let us discuss a practical use for the relationships derived above and give several examples that illustrate the results obtained by combining the DFT coefficients of the first and second contrasts.

At the beginning, let us consider test objects with similar shapes (Table 1). By analyzing the results of the Fourier transform of the test objects (Table 1, rows 1–5), it is possible to infer that the reconstructed contrasts reliably visualize objects resembling those of the contrasts used to create the arguments of the DFT coefficients. It should be emphasized that objects,

including those located at different points of the spatial region under analysis (Table 1, row 4), and even small details on the initial contrast (Table 1, row 5, where image elements are designated by arrows), are correctly recovered. The results from Table 1 clearly demonstrate that the phase is indeed most informative upon recovery of the shape, sizes, and geometric position of the object being analyzed.

At the same time, the reconstructed contrasts contain numerous interfering aperiodic artifacts. Moreover, the larger an object on the initial contrast, the clearer the artifacts that are on the recovered contrast. In addition, the artifacts undergo changes and their periods are shifted with respect to the image center if the objects are displaced inside the analyzed spatial region. Their appearance is caused by sharp boundaries between the object and the surrounding background, the existence of which is predicted by Fourier transform theory. Continuous broadening of the boundary-blurring region leads to the gradual disappearance of artifacts.

The aforementioned Fourier transform technique was also applied to test objects with completely different shapes (Table 1, rows 6, 7). The reconstructed images exhibited practically the same result as test objects with analogous shapes: the recovered images are comprised of elements of the contrasts used to specify the argument (phase) of DFT coefficients, although artifacts are manifested not as noticeably as compared to objects with identical and similar shapes.

In the analysis of experimental X-ray topographic and polarization-optical contrasts incorporating images of defects in a single-crystal structure, a situation is rather frequently met when defect rosettes of the same and different types are partially or fully overlapped. This greatly hinders the identification and separation of defects and their localization in the single-crystal bulk. In this context, it is of interest to apply the Fourier transform technique proposed above to test objects with partially overlapped elements whose shapes are similar to each other.

On the basis of the reconstructed contrasts, images of individual elements could not be revealed in an explicit form (in this case, recovery occurred using absolute values of the DFT coefficients of the contrast with partial element overlapping and the corresponding arguments of the contrast involving a single superimposed element). However, according to the indirect criterion consisting in the fact that the image of another superimposed element is symmetrically doubled with respect to the center of an element, which is revealed on the reconstructed contrast, defect identification is still possible (Table 2, rows 1, 2).

In the case where the Fourier transform is applied to centered test objects with similar shapes, different

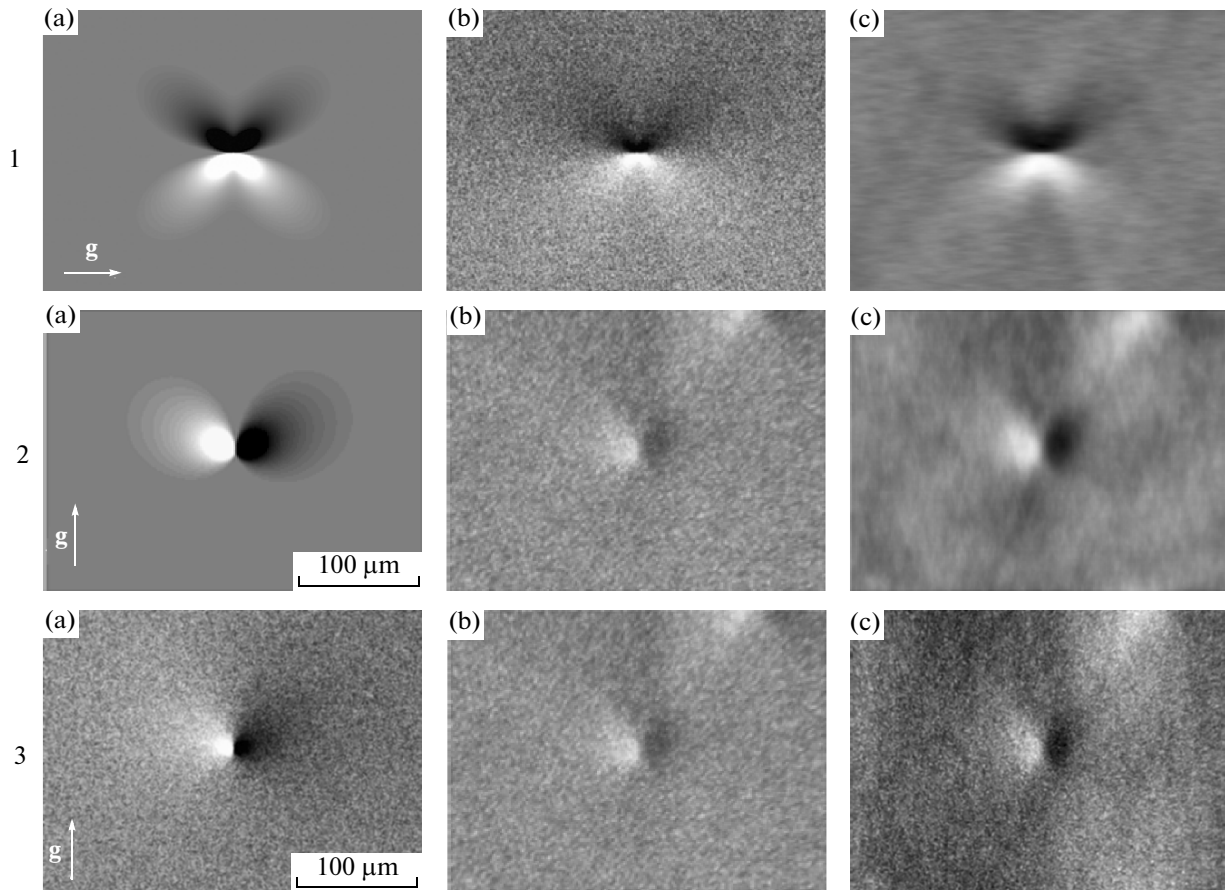


Fig. 2. Images of intensity rosettes around the (1) edge and (2, 3) screw dislocations in the silicon-carbide single crystal. Line 1 consists of (a) theoretical contrast and (b) noisy theoretical contrast, line 2 includes (a) theoretical contrast and (b) experimental contrast, and line 3 incorporates (a) noisy theoretical contrast and (b) experimental contrast. Lines 1–3 involve (c) images reconstructed with absolute values of the DFT coefficients of the contrast (a) and arguments of the DFT coefficients of the contrast (b).

sizes, and complete overlapping (Table 2, rows 3, 4), the reconstructed contrasts involve images resembling the initial one but with distorted artifacts. The image intensity of the element (the argument of the DFT coefficients of its contrast (contrast 2) were used during recovery) is closer to the initial contrast intensity. Moreover, the recovered image contains all distinctive features of the initial contrast.

Let us analyze the results of the Fourier transform of centered test objects with similar shapes, different sizes, and contrasts of different intensity under the condition of complete overlapping (Table 3, rows 1–3). The overlay includes four centered circles with different diameters and different intensity levels. The intensities are numbered from the periphery to the center (Fig. 1). From comparison between contrasts, the intensity-level step ΔI was fixed and took values from 25 to 1. The reconstruction process was implemented using (i) the unit absolute values of the DFT coefficients and (ii) the absolute values of the DFT coefficients of the contrast incorporating the image of one of

the superimposed circles. The results from Table 3 enable us to infer that, in reconstructing the contrast with unit absolute values and absolute values of the DFT coefficients of the image containing the circle of the largest diameter, the superimposed circle boundaries are observed only down to the intensity step $\Delta I = 15$. At the same time, the initial contrast makes it possible to identify the circle boundaries at an intensity step of $\Delta I = 5$. Moreover, the recovered contrast includes barely any artifacts. If recovery was based on the absolute values of the DFT coefficients for the image incorporating the circle of the least diameter, the reconstructed contrast would contain a significant number of artifacts, but the superimposed circle boundaries manifest themselves on the PC display even if the intensity step is $\Delta I = 1$. This is confirmed by intensity jumps inherent to the recorded intensity profiles (IPs) (Table 3, rows 4, 5).

In constructing the IPs of the images presented in Table 3, the horizontal coordinates N of pixels and the intensities I of gray gradation (0–255) were plotted on

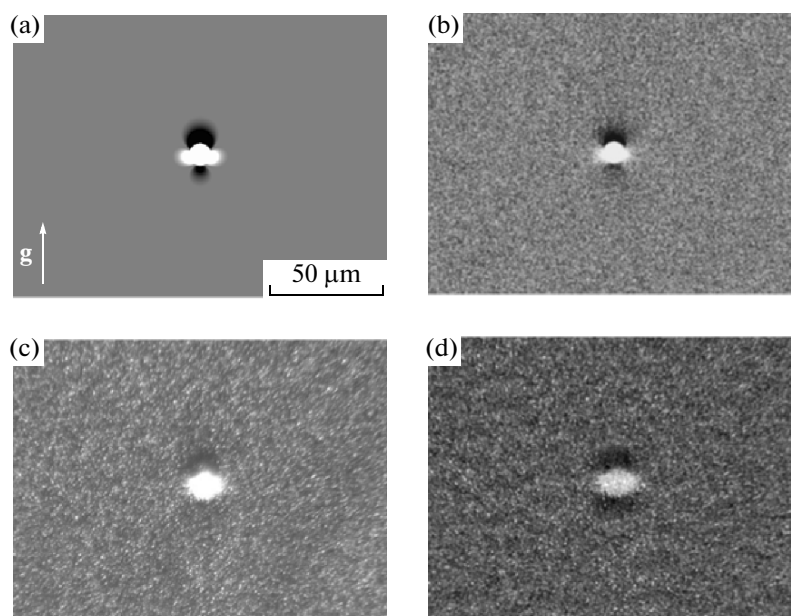


Fig. 3. Images of the intensity rosette around the embedded microdefect in a silicon-carbide single crystal: (a) theoretical contrast, (b) noisy theoretical contrast, (c) experimental contrast, and (d) rosette reconstructed with absolute values of the DFT coefficients of the contrast (b) and the arguments of the DFT coefficients of the contrast (c).

the abscissa and ordinate axes, respectively. The IPs were precisely recorded along the central horizontal line of all images from left to right.

ROLE OF THE ARGUMENT OF THE DFT COEFFICIENTS IN THE CASE OF THE FOURIER TRANSFORM OF AN EXPERIMENTAL CONTRAST

The Fourier-analysis approach discussed above can be employed to reconstruct a noisy theoretical contrast. The reconstruction process will be performed using absolute values of the DFT coefficients of the theoretical contrast and the arguments of the DFT coefficients of the noisy theoretical contrast (Fig. 2, line 1). Comparison between the initial (Fig. 2a) and recovered noisy (Fig. 2b) images indicates that the reconstructed image contains all of the basic features of the initial image (Fig. 2a) in the near and far regions; this is evidence of the fact that a defining role is played by the arguments of the DFT coefficients of the contrast.

Analogous results were also obtained via the proposed Fourier-transform technique as applied to experimental contrasts [10] (Fig. 2, lines 2, 3). For 6H-SiC single crystals, all experimental contrasts were measured using X-ray topography based on the Borrmann effect.

In the case of silicon-carbide single crystals, the recovered experimental contrasts provide higher-quality images of the intensity rosettes around structural defects (Fig. 2, images 2c, 3c; Fig. 3d; Figs. 4c–

4k), making it possible not only to determine the shape and sizes of the rosettes more accurately but also to identify the defect type and its localization in the bulk of the single-crystal sample under study. The contrast of intensity rosettes on the recovered images (Fig. 2, images 2c, 3c) can be qualitatively improved if reconstruction is performed using absolute values of the DFT coefficients of noise-free (Fig. 2, image 2a) and noisy (Fig. 2, image 3a) theoretical contrasts.

An interesting result was obtained in recovering the experimental contrast of the intensity rosette around an embedded microdefect in a silicon-carbide single crystal [10] (Fig. 3). In this case, the initial contrast was reconstructed using absolute values of the DFT coefficients of the contrast of the noisy theoretical intensity at a microdefect depth of $z = 0.2r_0$, where r_0 is the inclusion radius.

The recovered contrast (Fig. 3d) exhibits high symmetry of the upper and lower petals. This is evidence that the microdefect is closer to the surface than was expected.

The obtained result was employed to recover the experimental contrast of the intensity rosette around the embedded microdefect in the silicon-carbide single crystal (Fig. 4). This process was carried out using absolute values of the DFT coefficients for the contrast of the noisy theoretical intensity at a microdefect depth of $z = 0$ (Fig. 4b), $z = 0.2r_0$ (Fig. 4d), $z = 0.4r_0$ (Fig. 4f), $z = 1.7r_0$ (Fig. 4h), and $z = 2.6r_0$ (Fig. 4j). The intensity-rosette images on the reconstructed experimental contrasts are very alike (Figs. 4c–4g)

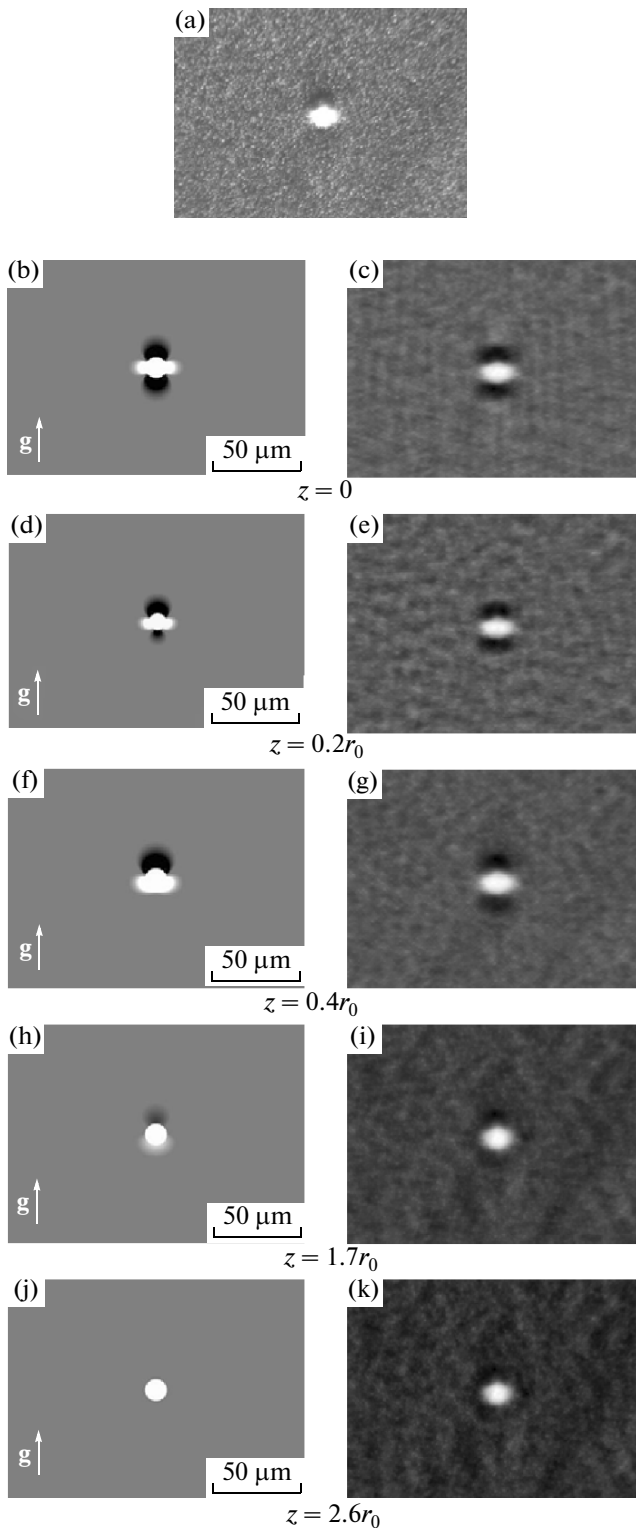


Fig. 4. Images of the intensity rosette around the embedded microdefect in a silicon-carbide single crystal: (a) experimental contrast, (b, d, f, h, j) theoretical contrasts with different microdefect depths, and (c, e, g, i, k) rosettes reconstructed with absolute values of the DFT coefficients of the contrasts (b, d, f, h, j) and the arguments of the DFT coefficients of the contrast (a).

even if the existence of artifacts is taken into account and confirm that the identified microdefect is always arranged closer to the surface. Moreover, from analysis of the results of the Fourier transform of the contrasts (Fig. 4), it can be asserted that a high similarity between the images of defects of the theoretical and experimental contrasts leads to a decrease in the number of artifacts in the reconstructed contrasts.

CONCLUSIONS

From analysis of the reconstructed test images and recovered theoretical and experimental contrasts containing images of the main types of structural defects, the following conclusions can be made:

(i) Basic information on the image structure is included in the arguments of discrete Fourier-transform coefficients.

(ii) The above-discussed Fourier analysis of topographic images, which is based on a combination of absolute values of the DFT coefficients of a theoretical contrast and arguments of the DFT coefficients of an experimental contrast under image reconstruction, enables the more reliable identification of a defect and its localization in the bulk of a single crystal.

(iii) The structural-defect identification technique, which was proposed in [9] and relies on simulating the noise-induced factors of a theoretical contrast and comparing the theoretical and experimental contrasts with subsequent digital processing, can be employed together with the Fourier transform. In so doing, arguments of the DFT coefficients of the experimental contrast and absolute values of the DFT coefficients of the theoretical contrast similar to that under analysis are chosen. Thus, there is no need for additional selection of the theoretical contrast.

Visually undefinable changes in the intensity of the reconstructed image are reliably fixed by quantitative criteria via the construction of intensity profiles and brightness characteristics.

Investigations of digital processing applied to topographic and polarization-optical images to improve their quality carried out previously [2, 10] make it possible to assume that discrete wavelet analysis can become an efficient tool for digitally processing experimental contrasts. This is explained by the fact that, as opposed to Fourier analysis which uses trigonometric basis, wavelet analysis involves a large packet of different short functions that can be adapted to solving the problems discussed above.

ACKNOWLEDGMENTS

This work was performed at the Computer Technologies in Diffraction Diagnostics of Materials scientific-educational laboratory, which was jointly created by the Veliky Novgorod Branch, St. Petersburg State University of Economics, Veliky Novgorod, and the

A. F. Ioffe Physical-Technical Institute, Russian Academy of Sciences, St. Petersburg.

REFERENCES

1. L. Danilchuk, A. Okunev, and V. Tkal, *X-ray Topography on Base of Bormann Effect* (LAP Lambert Academic, Saarbrücken, 2012).
2. V. A. Tkal, A. O. Okunev, and I. A. Zhukovskaya, *The Brightness and Frequency Analysis of Images of Structure Defects* (LAP Lambert Academic, Saarbrücken, 2012).
3. V. A. Bushuev and A. A. Sergeev, *Poverkhnost'*, No. 9, 48 (2000).
4. V. A. Bushuev and A. A. Sergeev, *Poverkhnost'*, No. 1, 52 (2003).
5. L. A. Zalmanzon, *The Fourier, Walsh, and Haar Transformations and Their Applications in Control, Communication, and Other Areas* (Nauka, Moscow, 1989) [in Russian].
6. V. P. D'yakonov, *Computer Mathematics. Theory and Applications* (Knowledge, Moscow, 2001) [in Russian].
7. Yu. E. Voskoboinikov, A. B. Gochakov, and A. B. Kolker, *Filtering of Signals and Images: Fourier and Wavelet Algorithms (with Examples in Mathcad)* (NGASU, Novosibirsk, 2010) [in Russian].
8. V. A. Bushuev, in *Proceedings of the 3rd International Scientific School-Seminar on Modern Methods of Diffraction Data Analysis (Diffraction Methods in Nanotechnologies)* (Novgor. Gos. Univ., Vel. Novgorod, 2011), p. 36.
9. V. A. Tkal, I. V. Dzyuba, and L. N. Danil'chuk, *J. Surf. Invest.: X-ray, Synchrotron Neutron Tech.* **3**, 797 (2009).
10. V. A. Tkal and I. A. Zhukovskaya, *Zavod. Lab., Diagn. Mater.*, No. 4, 28 (2013).

Translated by S. Rodikov